

19 **ABSTRACT**

20 How tick-borne pathogens interact with their hosts has been primarily studied in
21 vertebrates where disease is observed. Comparatively less is known about pathogen
22 interactions within the tick. Here, we report that *Ixodes scapularis* ticks infected with
23 either *Anaplasma phagocytophilum* (causative agent of anaplasmosis) or *Borrelia*
24 *burgdorferi* (causative agent of Lyme disease) show activation of the ATF6 branch of
25 the unfolded protein response (UPR). Disabling ATF6 functionally restricts pathogen
26 survival in ticks. When stimulated, ATF6 functions as a transcription factor, but is the
27 least understood out of the three UPR pathways. To interrogate the *Ixodes* ATF6
28 transcriptional network, we developed a custom R script to query tick promoter
29 sequences. This revealed *stomatin* as a potential gene target, which has roles in lipid
30 homeostasis and vesical transport. *Ixodes stomatin* was experimentally validated as a
31 bona fide ATF6-regulated gene through luciferase reporter assays, pharmacological
32 activators, and RNAi transcriptional repression. Silencing *stomatin* decreased *A.*
33 *phagocytophilum* colonization in *Ixodes* and disrupted cholesterol dynamics in tick cells.
34 Furthermore, blocking *stomatin* restricted cholesterol availability to the bacterium,
35 thereby inhibiting growth and survival. Taken together, we have identified the *Ixodes*
36 ATF6 pathway as a novel contributor to vector competence through Stomatin-regulated
37 cholesterol homeostasis. Moreover, our custom, web-based transcription factor binding
38 site search tool “ArthroQuest” revealed that the ATF6-regulated nature of *stomatin* is
39 unique to blood-feeding arthropods. Collectively, these findings highlight the importance
40 of studying fundamental processes in non-model organisms.

41 **Keywords:** *Ixodes scapularis*; *Anaplasma phagocytophilum*; *Borrelia burgdorferi*; tick-
42 borne disease; vector competence; unfolded protein response; ATF6; transcriptional
43 regulation; transcription factor binding; transcriptional network; Stomatin; cholesterol

44 **IMPORTANCE**

45 Host-pathogen interactions for tick-borne pathogens like *Anaplasma*
46 *phagocytophilum* (causative agent of Anaplasmosis) have been primarily studied in
47 mammalian hosts. Comparatively less is known about interactions within the tick.
48 Herein, we find that tick-borne pathogens activate the cellular stress response receptor,
49 ATF6, in *Ixodes* ticks. Upon activation, ATF6 is cleaved and the cytosolic portion
50 translocates to the nucleus to function as a transcription factor that coordinates gene
51 expression networks. Using a custom script in R to query the *Ixodes* ATF6 regulome,
52 *stomatin* was identified as an ATF6-regulated target that supports *Anaplasma*
53 colonization by facilitating cholesterol availability to the bacterium. Moreover, our
54 custom, web-based tool “ArthroQuest” found that the ATF6-regulated nature of *stomatin*
55 is unique to arthropods. Given that lipid hijacking is common among arthropod-borne
56 microbes, ATF6-mediated induction of *stomatin* may be a mechanism that is exploited
57 in many vector-pathogen relationships for the survival and persistence of transmissible
58 microbes. Collectively, this study identified a novel contributor to vector competence
59 and highlights the importance of studying molecular networks in non-model organisms.

60 INTRODUCTION

61 The North American deer tick, *Ixodes scapularis*, can transmit up to seven
62 different pathogens that impact human and animal health including *Anaplasma*
63 *phagocytophilum* (causative agent of Anaplasmosis) and *Borrelia burgdorferi* (causative
64 agent of Lyme Disease)¹. The continuous rise in reported cases of tick-borne disease²⁻
65 ¹⁰ underscores the need for novel intervention strategies. Although the intricacies of
66 mammalian host-pathogen interactions have been well-studied, comparatively little is
67 known about tick-pathogen interactions.

68 Recently we have shown that *A. phagocytophilum* and *B. burgdorferi* activate the
69 unfolded protein response (UPR) in ticks, which influences microbial colonization and
70 persistence in the arthropod^{11,12}. The UPR is a cellular response network that is initiated
71 by three endoplasmic reticulum (ER) transmembrane receptors IRE1 α , PERK, and
72 ATF6. Each branch of the UPR initiates a signaling cascade and coordinates gene
73 expression networks by activating specific transcription factors. We have shown that the
74 IRE1 α -TRAF2 pathway leads to microbe-restricting immune responses in arthropods by
75 activating the NF- κ B-like molecule, Relish¹¹. We have also demonstrated that
76 stimulating PERK activates the antioxidant transcription factor, Nrf2, which facilitates
77 pathogen persistence in ticks¹². Out of the three UPR receptors, ATF6 is the least
78 understood¹³. When activated, site-1 and site-2 proteases cleave the cytosolic portion of
79 ATF6, which allows it to translocate to the nucleus and act as a transcriptional regulator
80 (nATF6)¹⁴. The role of ATF6 has never been explored in arthropod vectors.

81 Here, we demonstrate that *Ixodes* ATF6 is activated by tick-borne pathogens and
82 supports *A. phagocytophilum* colonization in ticks. To determine how ATF6 impacts

83 vector competence, we used protein modeling and a custom transcription factor binding
84 site query to probe the ATF6 regulatory network in *I. scapularis*. Gene ontology (GO)
85 and Reactome analyses identified Stomatin, a lipid homeostasis and vesical transport
86 protein, as a potential gene regulated by ATF6 in ticks. Using pharmacological
87 manipulations, RNA interference (RNAi), and quantitative fluorescent assays, we found
88 that Stomatin supports pathogen colonization in ticks by facilitating cholesterol
89 acquisition by the bacterium. These findings demonstrate that *stomatin* is induced
90 during the arthropod-phase of the pathogen life cycle to enable survival and persistence
91 in the vector.

92 Programs that predict transcription factor regulatory networks are generally
93 restricted to model organisms, leaving out many arthropod vectors. We used our
94 custom R script to develop a publicly available, web-based tool termed “ArthroQuest”
95 that currently allows users to query 20 different arthropod vector genomes, in addition to
96 *Drosophila* and humans. Queries with ArthroQuest revealed that the ATF6-regulated
97 nature of *stomatin* appears to be unique to arthropods. Given that lipid hijacking and
98 cholesterol incorporation is common in many arthropod-borne microbes¹⁵, ATF6-
99 mediated induction of *stomatin* may be a shared phenomenon among many vector-
100 pathogen relationships that is exploited for the survival and persistence of transmissible
101 pathogens.

102

103 **RESULTS**

104 *ATF6 is induced by tick-borne pathogens and supports microbial survival*

105 Previously, we found that *A. phagocytophilum* and *B. burgdorferi* activate the
106 UPR through ER receptors IRE1 α and PERK, which influence bacterial colonization of
107 the tick^{11,12}. The UPR coordinates a variety of transcription factors that modulate the
108 expression of genes involved in cellular stress responses, immunity, and several other
109 physiological conditions^{16–18}. To determine which UPR-associated transcription factors
110 respond to infection, we employed a surrogate luciferase reporter plasmid assay¹² and
111 found that ATF6 was significantly activated by both *A. phagocytophilum* and *B.*
112 *burgdorferi* (Fig 1A-B). We next asked if *atf6* is induced in ticks during infection. *I.*
113 *scapularis* larvae were fed to repletion on either *A. phagocytophilum* or *B. burgdorferi*-
114 infected mice and gene expression was analyzed by quantitative real-time PCR (qRT-
115 PCR). In both groups of infected larvae, *atf6* expression was significantly increased (Fig
116 1C-D). To determine how this may impact pathogen colonization, we silenced *atf6* in
117 tick cells using RNAi prior to infecting with *A. phagocytophilum* and found that knocking
118 down *atf6* reduced bacterial survival and replication in tick cells (Fig 1E-F). Collectively,
119 this indicates that ATF6 is activated during infection and supports pathogen survival.

120

121 *Identifying genes putatively regulated by ATF6 in ticks*

122 Out of the three UPR pathways, ATF6 and the gene network it coordinates is the
123 least understood¹³. To examine how ATF6 is mechanistically impacting pathogen
124 dynamics in the tick, we first aligned sequences from *I. scapularis* and humans. We
125 found that, although there was low overall conservation (31.56% identity), there was
126 good conservation in the basic leucine zipper (bZIP) domain which is the DNA-
127 interacting portion of ATF6 (Supplementary Fig 1A; Supplementary Table 1). Moreover,

128 the amino acid residues defined as “essential for DNA binding”, K304, N305, and R306,
129 were 100% conserved between the two sequences¹⁹. We next used AlphaFold to
130 predict the protein structure of *Ixodes* ATF6 and then aligned it with the human
131 structure^{20,21} using ChimeraX²² (Fig 2A, Supplementary Fig 1B). We found that the bZIP
132 domain was structurally well-conserved and that the DNA-binding amino acid residues
133 were found in the same orientation between the two proteins (Fig 2B).

134 The conservation in DNA-binding domain structure and residues between
135 humans and ticks provided the impetus to interrogate the *Ixodes* genome for ATF6-
136 regulated genes. Non-model organisms, such as ticks, have a limited number of
137 genome and proteome analysis tools. Moreover, the tools that are available are often
138 not well-developed. To circumvent this issue, we created a custom query in R to search
139 for ATF6-regulated genes in *I. scapularis* (Fig 2C). Predicted promoter regions in the *I.*
140 *scapularis* genome were defined as 1,000 base pairs upstream from all coding regions.
141 We then searched for ATF6-binding motifs in all promoters. ATF6 functions as a
142 homodimer that promotes gene expression either by itself or in combination with the
143 general transcription factor NF-Y (nuclear transcription factor Y). By itself, ATF6 can
144 drive gene expression by binding TGACGTG within a promoter sequence¹⁹. In
145 combination, ATF6 and NF-Y can drive transcription by binding CCACG and CCAAT,
146 respectively^{23,24}. We scanned all predicted *Ixodes* promoters for either TGACGTG or
147 CCACG in the presence of CCAAT. For comparison, we also predicted ATF6-binding
148 sites in humans and the model insect *D. melanogaster*. Genes downstream from
149 promoters containing ATF6-binding sites were compiled, identified, and compared (Fig
150 2D; Supplementary Table 2). This revealed that known ATF6-regulated genes, including

151 *binding immunoglobulin protein (BiP)* and *x-box binding protein 1 (xbp1)*, were present
152 in all three organisms, demonstrating that our custom R script correctly identifies ATF6-
153 regulated genes. We also observed that more genes were shared between *Ixodes* and
154 *Drosophila* (866) than humans and *Ixodes* (290), but the large majority of genes were
155 unique to each organism (Fig 2D).

156 We next sought to analyze the ATF6-regulated gene network in ticks. However,
157 when compared to humans or *Drosophila*, relatively little gene information is available
158 for *Ixodes*. To overcome this obstacle, we identified human and *Drosophila* orthologs for
159 tick gene targets and then extracted corresponding gene information (Supplementary
160 Table 2). 71% of the *Ixodes* genes putatively regulated ATF6 mapped to human and/or
161 *Drosophila* orthologs. Corresponding Gene Ontology (GO) and Reactome information²⁵⁻
162 ²⁷ were used to perform pathway enrichment analysis²⁸ (Supplementary Fig 2), which
163 revealed that GO terms associated with the UPR were enriched (Supplementary Table
164 3). This also returned categories of interest with the potential to impact microbial
165 colonization including “Immunity”, “Positive Regulation of Bacterial or Viral Processes”,
166 “Signal Transduction”, and “Associated with the ER”^{14,29}. From *Ixodes*, we found 185
167 genes associated with Immunity (GO:0006955, R-HSA-768256), 24 with Positive
168 Regulation of Bacterial or Viral Processes (GO:0048524, GO:1900425), 181 with Signal
169 Transduction (R-HSA-162582), and 179 Associated with the ER (GO:0005783) (Fig
170 2E). The genes *stomatin*, *neurogenic locus notch homolog protein 1 (notch1)*, and
171 *protein disulfide isomerase (pdi)* were found in all four GO categories. *Pdi* is a known
172 ATF6-regulated gene in mammals and assists in the formation of disulfide bonds³⁰.
173 *Notch1* is also known to be regulated by ATF6 and is involved in immunity, cellular

174 development, and apoptosis^{31,32}. Stomatin has roles in lipid homeostasis and vesical
175 transport³³, but has never been linked to ATF6. Since *A. phagocytophilum* incorporates
176 lipids and cholesterol into its membrane, we hypothesized that regulation of *stomatin*
177 expression could be how ATF6 is supporting *A. phagocytophilum* in ticks.

178

179 *Tick stomatin is upregulated by ATF6 during infection*

180 We next used AlphaFold³⁴ to predict structural interactions between ATF6 and
181 the *stomatin* promoter (Fig 3A; Supplementary Fig 3A). We found that the *Ixodes* ATF6
182 homodimer (Fig 3A, tan) and DNA-interacting residues K304, N305, and R306 (Fig. 3A,
183 purple) were predicted to be in direct contact with the ATF6-binding nucleotide motif
184 found in the *stomatin* promoter, CCACG (Fig 3A, yellow). To test whether ATF6
185 activation increases *stomatin*, we used a drug, AA147, that selectively activates ATF6
186 independent of ER stress³⁵. AA147 did not impact cell viability (Supplementary Fig 3B),
187 but did cause a dose-dependent increase in *stomatin* expression (Fig 3B). Since
188 pharmacological manipulators can have off-target effects, we also silenced *atf6* in tick
189 cells using RNAi. We found that decreasing *atf6* levels (Fig 1E) caused a significant
190 decline in *stomatin* expression (Fig 3C), altogether demonstrating that ATF6 positively
191 correlates with *stomatin* expression.

192 To experimentally validate that ATF6 binds the *stomatin* promoter and drives
193 expression, we designed a Luciferase reporter assay. First, we cloned the *Ixodes*
194 *stomatin* promoter upstream from a *luciferase* gene. Next, plasmids were constructed
195 that constitutively expressed recombinant versions of *Ixodes* nATF6 and NF-Y
196 (Supplementary Fig 4A-4B). All three plasmids were then co-transfected into HEK 293T

197 cells for 24 hours (Fig 3D). A positive control plasmid containing *luciferase* driven by an
198 *atf6* promoter was also co-transfected with *Ixodes* nATF6 and NF-Y constructs
199 (Supplementary Fig 4C). After 24 hours, D-luciferin was added to the cells and
200 Luciferase activity was assayed. We found a significant increase in Luciferase activity
201 when cells were expressing both *Ixodes* nATF6 and NF-Y, indicating *stomatin* promoter
202 activity (Fig 3D). Altogether, these data demonstrate that ATF6, in combination with the
203 ubiquitously expressed transcription factor NF-Y, positively regulates the expression of
204 *stomatin* in *Ixodes* ticks.

205 We next evaluated *in vivo stomatin* expression in infected ticks. *Stomatin* was
206 quantified in larvae that had been fed on either *A. phagocytophilum* (Fig 3E) or *B.*
207 *burgdorferi* (Fig 3F) infected mice, and then rested for 7 days or 14 days post-repletion,
208 respectively. This time period correlates with the expansion of microbes in the tick post-
209 repletion³⁶. We also quantified *stomatin* expression in *A. phagocytophilum* or *B.*
210 *burgdorferi* infected, flat nymphs (Fig 3G). From both life stages, we found that ticks
211 infected with *A. phagocytophilum* had elevated levels of *stomatin* expression when
212 compared to uninfected ticks. Ticks infected with *B. burgdorferi* had no differences at
213 the rested larval stage, but significantly increased levels of *stomatin* at the unfed nymph
214 stage. It is not clear why *stomatin* is induced in *A. phagocytophilum*-infected, rested
215 larvae, but not *B. burgdorferi*. It is possible that differences in niche colonization and
216 subcellular location between the two pathogens are responsible for this observation.
217 This data, together with infection-induced ATF6 transcriptional activity (Fig 1D)
218 demonstrates that ATF6 positively regulates *stomatin* during *A. phagocytophilum* and *B.*
219 *burgdorferi* infection in ticks.

220

221 *Arthropod infection is supported by stomatin*

222 Since Stomatin expression increased with *A. phagocytophilum* acquisition in
223 ticks, we next asked what impact it has on microbial colonization. To address this, we
224 used RNAi to silence *stomatin* in tick cells prior to infecting with *A. phagocytophilum*.
225 We found that blocking *stomatin* expression caused a decrease in *Anaplasma* numbers
226 (Fig 4A), similar to what was observed when silencing *atf6* (Fig 1E). To determine how
227 Stomatin impacts microbial colonization *in vivo*, we immersed *Ixodes* larvae^{11,12} in
228 siRNA targeting *stomatin*. Ticks were then allowed to feed to repletion on *A.*
229 *phagocytophilum*-infected mice. We found a 2-fold decrease in *Anaplasma* numbers
230 when *stomatin* expression was knocked down relative to the scrambled control (Fig 4B),
231 demonstrating that *A. phagocytophilum* infection and colonization of ticks is supported
232 by Stomatin.

233

234 *Stomatin supports cholesterol incorporation into Anaplasma*

235 Stomatin is a member of the stomatin/prohibitin/flotillin/HflK/C (SPFH) family
236 found in lipid rafts on cell membranes, lipid droplets, and endosomes and is known to
237 be involved in vesicle trafficking³⁷. When comparing human and *Ixodes* Stomatin, we
238 found that the amino acid sequences and structures are well conserved (Supplementary
239 Fig 5A-C). The *Ixodes* Stomatin SPFH domain (residues 32-191) contains four
240 cholesterol recognition/interaction amino acid consensus sequences, CRAC and CARC
241 (Fig 4C, pink; Supplementary Fig 5D)³⁸. Outside of the SPFH domain, there are two

242 additional CARC domains. This suggests that tick Stomatin may bind cholesterol and
243 function similarly to other SPFH family members³⁷.

244 Cholesterol is essential to the development of *A. phagocytophilum* infection³⁹. In
245 mammals, *A. phagocytophilum* will intercept free cholesterol from the low-density
246 lipoprotein uptake pathway³⁹ and incorporate it for structural support of its membrane.
247 We therefore asked if *A. phagocytophilum* impacts cholesterol dynamics in ticks. Using
248 an Amplex Red cholesterol assay, cholesterol was quantified in uninfected tick cells
249 relative to tick cells that were persistently infected with *A. phagocytophilum*. We found
250 that infection was associated with significantly more cholesterol compared to uninfected
251 cells, indicating that *Anaplasma* induces cholesterol accumulation in ticks (Fig 4D).

252 SPFH-domain containing proteins regulate cholesterol uptake, distribution within
253 the cell, and exportation when levels become too high^{40,37}. To understand how Stomatin
254 may be impacting cholesterol dynamics within tick cells, we transfected silencing RNAs
255 targeting *stomatin* into uninfected cells and then quantified cholesterol. We found that
256 when *stomatin* expression is reduced there is an increase in total cholesterol, implying
257 that Stomatin is involved in proper distribution, localization, and export of cholesterol
258 from the cell (Fig 4E).

259 Given the *Anaplasma*-supporting role that Stomatin plays, we asked if it could be
260 facilitating infection and colonization by shuttling cholesterol to the bacterium. To
261 address this possibility, we silenced *stomatin* in persistently infected tick cells for five
262 days (Supplementary Fig 5E). *A. phagocytophilum* were then mechanically lysed from
263 tick cells, washed, and separated from host cell debris. Bacterial cholesterol levels were
264 then quantified using the Amplex Red cholesterol assay. We found that when *A.*

265 *phagocytophilum* is grown in cells with depleted Stomatin, there is significantly less total
266 cholesterol incorporated into the bacteria compared to non-silenced controls (Fig 4F).
267 Therefore, although knocking down *stomatin* caused increased total cellular cholesterol
268 in tick cells, our data shows that it is not accessible by *Anaplasma*. This finding depicts
269 a model where *Anaplasma* activates ATF6 in *Ixodes*, which upregulates Stomatin
270 expression and functionally supports the microbe by facilitating cholesterol delivery,
271 likely for cell wall structure and growth (Fig 5A).

272

273 *ArthroQuest: ATF6-regulation of stomatin is unique to arthropod vectors*

274 Programs that predict transcription factor regulatory networks have generally
275 been restricted to model organisms, leaving out most arthropod vectors^{41,42}. To address
276 this deficiency, we created a web-based tool termed “ArthroQuest” to serve as a
277 resource for the vector biology community
278 (<https://datahub.vetmed.wsu.edu/Shaw/ArthroQuest/>). This tool can query 22 pre-
279 loaded arthropod vector genomes for transcription factor binding motifs. Pre-loaded
280 genomes include those from ticks, mosquitoes, lice, sand flies, mites, fleas, *Drosophila*,
281 and humans. Using NCBI genomic FASTA and annotation files, we defined promoter
282 regions for all 22 genomes and created a user-friendly interface with Shiny App. Users
283 can enter a DNA-binding motif of interest and then select a genome to query. Annotated
284 genes found downstream from positive-hit promoter regions can then be downloaded as
285 a table. Using this tool, we queried all pre-loaded genomes for ATF6-binding sites. In
286 contrast to humans, the large majority of arthropods (18 out of 21) had positive hits in
287 the promoter regions of *stomatin* orthologs, including other ticks, mosquitos, and sand

288 flies (Fig 5B, Supplementary Table 4). Altogether, these findings suggest that the ATF6-
289 regulated nature of *stomatin* may be a common feature among blood-feeding
290 arthropods.

291

292 **DISCUSSION**

293 Pathogen persistence in vectors can be attributed to both microbe and host-
294 responses, although the underlying mechanisms orchestrating this remain incompletely
295 understood. Recently, the UPR receptors IRE1 α and PERK have been connected to
296 arthropod immunity and vector competence of ticks^{11,12}. The third pathway orchestrated
297 by ATF6 remains the least understood out of the UPR circuits¹³. In this article, we show
298 that transmissible pathogens *A. phagocytophilum* and *B. burgdorferi* activate ATF6 in *I.*
299 *scapularis*, which supports pathogen colonization and persistence in the tick. We
300 provide evidence that the ATF6-regulated transcriptional network supports pathogen
301 survival by inducing Stomatin, which facilitates cholesterol delivery to the bacterium.
302 Moreover, queries using our custom, web-based transcription factor binding site tool
303 ArthroQuest suggest that the ATF6-regulated nature of *stomatin* is unique to
304 arthropods. Collectively, our findings provide mechanistic insight into how cellular stress
305 responses influence vector competence of arthropods and further highlight the
306 fundamental differences in molecular networks between mammals and ticks.

307 To our knowledge, this is the first study to mechanistically investigate how ATF6
308 influences pathogen dynamics in an arthropod vector. The ATF6 regulatory network
309 controls the expression of genes involved in maintaining protein homeostasis, misfolded
310 protein degradation^{16,43}, development, tissue homeostasis, and cytoprotection^{14,43}. Our

311 R script querying the *I. scapularis* genome not only predicted known ATF6-regulated
312 genes, but also many others that have not been previously implicated in the ATF6
313 regulome. This approach led us to the novel finding that ATF6 transcriptionally regulates
314 tick *stomatin*. In addition to *stomatin*, there are several other genes that are unique to
315 the *Ixodes* ATF6 regulome that are not yet characterized (Supplementary Table 2). How
316 these unique targets may be impacting vector competence is an area for future study.

317 ATF6 has previously been connected to lipid metabolism in mammals⁴⁴. *Ixodes*
318 ticks only feed once per life stage and must adapt to an influx of proteins and lipids
319 when taking a blood meal, which can confer stress to the tick¹⁶. It is possible that stress-
320 responses are activated during blood feeding and that the ATF6-regulated nature of
321 *stomatin* in ticks is needed for the proper coordination of lipid homeostasis and
322 metabolism. Increased Stomatin expression could stabilize lipid rafts, improve
323 membrane integrity, and/or protect the cell membrane against oxidative stress that is
324 associated with a blood meal. This linkage between ATF6 and lipid homeostasis
325 through Stomatin in arthropods may be something that vector-borne pathogens target
326 and actively manipulate to satisfy their own cholesterol requirements for growth and
327 survival¹⁵.

328 Our script in R led to the development of a customizable tool, ArthroQuest, to
329 predict transcription factor binding sites in non-model arthropods
330 (<https://datahub.vetmed.wsu.edu/Shaw/ArthroQuest/>). Other tools, such as Transfac or
331 TFtarget, exist but are only available for model organisms^{41,45}. In addition to humans
332 and *Drosophila*, ArthroQuest currently allows users to query 20 different arthropod
333 vector genomes. This led to the finding that humans do not have an ATF6 binding site in

334 the predicted promoter region of *stomatin*, but the large majority of vectors genomes on
335 ArthroQuest do. This includes several other species of ticks, mosquitos, and sandflies,
336 which suggests that ATF6-mediated regulation of *stomatin* could be a common
337 phenomenon among blood-feeding arthropods. When considering the rapid nutrient
338 influx and temperature shift that hematophagous arthropods endure during blood
339 feeding, a stress-sensing network to cue lipid metabolism would be evolutionarily
340 advantageous, particularly if Stomatin influences cholesterol homeostasis and/or
341 membrane fluidity^{33,37,46,47}.

342 As a lipid-raft associated protein, Stomatin performs several functions within the
343 cell. It has been implicated in the host cell immune response to fungal pathogens by
344 assisting phagolysosome fusion⁴⁸. Despite this association with immunity, Stomatin has
345 also been shown to promote viral infection. For example, Stomatin assists Hepatitis C
346 virus (HCV) replication by supporting assembly of the viral RNA replicase complexes on
347 detergent-resistant membrane structures⁴⁹. Our study is the first to link Stomatin to
348 bacterial infection and replication. Previous reports have found that another SPFH
349 family protein, Flotillin, facilitates cholesterol transport to the *Anaplasma*-containing
350 vacuole in mammalian cells^{50,51}. Our findings show that Stomatin-depleted tick cells
351 have increased cholesterol accumulation within the cells, but decreased cholesterol
352 delivery to the bacterium, suggesting that the role of *Ixodes* Stomatin during *Anaplasma*
353 infection could be similar to mammalian Flotillin. This finding highlights that while the
354 cholesterol requirement for *Anaplasma* growth is conserved between mammalian and
355 tick environments, the molecular host targets that facilitate this process are distinct
356 between the two organisms.

357 While our findings show that both *A. phagocytophilum* and *B. burgdorferi*
358 infection activate ATF6 transcriptional activity, a recent study reported that ATF6 is not
359 activated in RF/6A cells during *Anaplasma* infection⁵². The discrepancy in results may be
360 attributable to differences in cell types and/or experimental approaches used to test for
361 ATF6 activation. Wang *et al.* used a transfected RF/6A cell line expressing recombinant,
362 GFP-tagged ATF6 and nuclear accumulation was assessed by fluorescence
363 microscopy after infection⁵². Our assay used a Luciferase reporter plasmid to
364 quantitatively detect transcriptional activity by endogenous, activated ATF6 in infected
365 HEK 293T cells. Another report observed an increase in cleaved ATF6 by immunoblot
366 in *A. phagocytophilum*-infected THP-1 cells, which also suggests activation⁵³. It is
367 possible that ATF6 activation may vary between stages of infection. For example, our
368 group previously reported that there was no difference in *atf6* transcript levels between
369 uninfected and *Anaplasma*-infected *Ixodes* nymphs immediately post-repletion¹¹.
370 However, in infected larvae that were rested for 7 days post-repletion, we found
371 increased *atf6* expression (Fig 1C-D). The discrepancy in expression at different
372 timepoints post-repletion could indicate that ATF6 is only activated after *Anaplasma* has
373 established infection and expanded in population within the tick. This hypothesis is in
374 line with our findings that ATF6 facilitates cholesterol delivery to the *Anaplasma*-
375 containing vacuole for bacterial growth and survival.

376 Many vector-borne pathogens are reliant on host cholesterol for membrane
377 structure and growth. For example, *B. burgdorferi*, *Ehrlichia* spp., and *Anaplasma* spp.
378 incorporate cholesterol into their outer membranes for structural integrity. Other vector-
379 borne parasites and viruses, such as *Plasmodium* spp. and flaviviruses, are also reliant

380 on host lipids for survival¹⁵. Based on this knowledge and the data presented herein, we
381 hypothesize that ATF6-regulation of Stomatin expression is a mechanism used by a
382 wide variety of blood-feeding arthropods to control lipid homeostasis during times of
383 stress, which is exploited by vector-borne pathogens to effectively colonize arthropods.

384

385 **METHODS**

386 *Cell culture.*

387 The *I. scapularis* embryonic ISE6 cells (received as gift from Ulrike Munderloh)
388 were cultured at 32°C with 1% CO₂ in L15C300 media supplemented with 10% heat-
389 inactivated FBS (Sigma, F0926), 10% tryptose phosphate broth (BD, B260300) and
390 0.1% lipoprotein bovine cholesterol (MP Biomedicals, 219147680).

391 The human embryonic kidney cell line, HEK 293T cells were cultured in flasks
392 (Corning, 353136) at either 33°C or 37°C in 5% CO₂ in Dulbecco's modified Eagle
393 medium (DMEM; Sigma, D6429) supplemented with 10% heat-inactivated FBS (Atlanta
394 Biologicals, S11550) and 1x Glutamax (Gibco, 35050061).

395

396 *Bacteria and animal models.*

397 *A. phagocytophilum* strain HZ was cultured in HL60 cells (ATCC, CCL-240) in
398 Roswell Park Memorial Institute 1640 (Cytiva SH30027.LS) medium supplemented with
399 10% heat-inactivated FBS and 1x Glutamax. Cultures were kept between 1 x 10⁵ and 1
400 x 10⁶ cells mL⁻¹ and maintained at 37°C in the presence of 5% CO₂. Persistently
401 infected ISE6 cells were cultured in L15C300 media supplemented with 25 µM 4-(2-
402 Hydroxyethyl)piperazine-1-ethane-sulfonic acid (Sigma, H4034-100G), 0.25% sodium

403 bicarbonate (Sigma, S-5761), pH 7.5 in unvented flasks (GeneseeSci, 25-207) at 37°C,
404 5% CO₂. *A. phagocytophilum* counts were performed as previously described^{11,54}. Host
405 cell-free *A. phagocytophilum* was isolated by syringe lysis with a 27-gauge needle.

406 *B. burgdorferi* B31 (strain MSK5) was grown in modified Barbour-Stoener-Kelly
407 II (BSK-II) medium supplemented with 6% normal rabbit serum (NRS; Pel-Freez;
408 31126-5) at 37°C, 5% CO₂. Dark-field microscopy was used to monitor the density and
409 growth phase of the spirochetes. Plasmid profiles of *B. burgdorferi* cultures were
410 screened by PCR before infection⁵⁵.

411 *Escherichia coli* cultures were grown overnight at 37°C with shaking between 230
412 and 250 rpm in lysogeny broth (LB) supplemented with 100 µg µl⁻¹ ampicillin.

413 *Ixodes scapularis* ticks were acquired at the larval stage from either the
414 Biodefense and Emerging Infectious Diseases Research Resources Repository for the
415 National Institute of Allergy and Infectious Disease at the National Institutes of Health
416 (<https://www.beiresources.org/>) or from Oklahoma State University (Stillwater, OK,
417 USA). Ticks were maintained with 16:8-h light:dark photoperiods and 95-100% relative
418 humidity at 23°C.

419 Male C57BL/6 mice were obtained from colonies at Washington State University
420 at ages six to ten weeks old. For *A. phagocytophilum* infection experiments, mice were
421 infected intraperitoneally with 1 x 10⁷ host cell-free bacteria in 100 µl of PBS
422 (Intermountain Life Sciences, BSS-PBS) as previously described^{11,54}. *A.*
423 *phagocytophilum* burdens of each mouse were assessed six days post-infection by
424 collecting 25 to 50 µl of blood from the lateral saphenous vein, as previously
425 described^{11,12}. *A. phagocytophilum* burdens were quantified by quantitative PCR (16s

426 relative to mouse β -actin). For *B. burgdorferi* infections, mice were inoculated
427 intradermally with 1×10^5 low-passage spirochetes. Seven days post-infection, blood
428 was collected from the lateral saphenous vein of each mouse and subcultured in BSK-II
429 medium. The presence of spirochetes were confirmed by dark field microscopy^{11,12}. All
430 experiments with mice were carried out according to the guidelines and protocols that
431 are approved by the American Association for Accreditation of Laboratory Animal Care
432 (AAALAC) and by the Office of Campus Veterinarian at Washington State University
433 (Animal Welfare Assurance A3485-01). The mice were housed in an AAALAC-
434 accredited facility at Washington State University in Pullman, WA. The Washington
435 State University Biosafety and Animal Care and Use Committees approved all
436 procedures.

437

438 *RNAi silencing and pharmacological treatments.*

439 The Silencer siRNA Construction Kit (Invitrogen, AM1620) was used to
440 synthesize silencing RNAs (siRNA) and scrambled RNAs (scRNA). For RNAi
441 knockdown experiments, ISE6 cells were seeded at 1×10^6 cells per well in a 24-well
442 tissue culture plate. siRNA or scRNA (3 μ g) were transfected into tick cells with 2.5 μ l of
443 Lipofectamine 3000 (Invitrogen, L3000008) for 24 hours. Plates were centrifuged at
444 room temperature for 1 hour at 450 x g and then incubated overnight. The following day,
445 cells were infected with *A. phagocytophilum* (MOI 50) for 18 hours. Cells were collected
446 in TRIzol (Invitrogen, 15596026) for RNA isolation. The Direct-zol RNA Microprep Kit
447 (Zymo; R2062) was used to extract RNA. cDNA was synthesized using the Verso cDNA
448 Synthesis Kit (Thermo Fisher Scientific; AB1453B) using 300 to 500 ng total RNA per

449 reaction. Gene silencing, bacterial burden, and gene expression were assessed by
450 quantitative reverse transcription PCR (qRT-PCR) with iTaq universal SYBR Green
451 Supermix (Bio-Rad, 1725125) (Supplementary Table 5). Cycling conditions were as
452 recommended by the manufacturer.

453 For pharmacological experiments, ISE6 cells were seeded at 1×10^6 cells per
454 well in a 24-well tissue culture plate and treated with 5-50 μM of AA147 (Focus
455 Biomolecules, 10-3973) for 24 hours. RNA isolation, cDNA synthesis, and qRT-PCR
456 were performed as described above. All data are expressed as means \pm standard error
457 of the mean (SEM).

458

459 *Protein structure predictions and alignments.*

460 *Ixodes* ATF6 and *Ixodes* NF-Y were identified using National Center for
461 Biotechnology Information protein Basic Local Alignment Tool (BLAST) and querying
462 the tick genome with human protein sequences (ATF6: AAB64434.1. NY-F:
463 ALX00018.1). All protein alignments were visualized with JalView⁵⁶. Shading indicates
464 physiochemical property conservation between amino acids. AlphaFold was used to
465 model *Ixodes* ATF6 and *Ixodes* Stomatin^{20,21}. Alignments with human orthologs were
466 performed in UCSF ChimeraX²². *Ixodes* ATF6 binding to the *Ixodes stomatin* promoter
467 was predicted using AlphaFold3 and visualized in ChimeraX³⁴. Sequences used for
468 AlphaFold predictions are found in Supplementary Table 1.

469

470 *Predicting ATF6 binding sites in the tick genome.*

471 All binding site analyses were conducted using R version 4.2.2 and RStudio
472 2022.07.2.576^{57,58}. The *I. scapularis* genome (GCF_01692078) was obtained from the
473 NCBI database in General Feature Format (GFF) and FASTA format⁵⁹. Putative
474 promoter sites were defined as the region 1000 base pairs upstream from each gene.
475 Coding domain sequence (CDS) coordinates from the GFF file were used to identify
476 promoter end sites. Promoter start sites were identified as 1000 nucleotides from the
477 promoter end site on both sense and antisense DNA strands. Using Biostrings⁶⁰ and
478 seqinR⁶¹ packages, the nucleotide sequence of each of the predicted promoter regions
479 was obtained from the FASTA file. Using the stringR package⁶², ATF6 binding sites
480 within predicted promoter sites were detected using the following motifs: TGACGTG
481 and CCACG with CCAAT. The resulting data included predicted promoter site
482 coordinates and the corresponding gene annotation. To create ArthroQuest, the R script
483 described above was reformatted to create a user-friendly interface with the R package
484 shiny⁶³.

485 To identify orthologs to the putatively ATF6-regulated genes, corresponding
486 protein accession numbers were used to find amino acid sequences from the *I.*
487 *scapularis* genome using the Rentrez package⁶⁴. Human (GCF_000001405.4) and
488 *Drosophila* (GCF_000001215.4) proteome files were obtained from NCBI as FASTA
489 files. Using the rBLAST package⁶⁵, each protein of interest was queried against human
490 or *Drosophila* proteins. The top 2 hits for each protein of interest were retrieved. All R
491 scripts are available in the GitHub repository ([https://github.com/Shaw-Lab/Vosbigian-](https://github.com/Shaw-Lab/Vosbigian-et-al-2025)
492 [et-al-2025](https://github.com/Shaw-Lab/Vosbigian-et-al-2025))
493

494 *Gene Enrichment Analysis Visualization.*

495 For pathway analysis, ortholog accessions were queried in Gene Ontology and
496 Reactome databases^{25–27}. Using the enrichplot package⁶⁶, pathways that were
497 significantly represented (Supplementary Table 3) were plotted. Adjusted *P*-value is
498 indicated by color, Ratios of enriched genes per total annotated genes are indicated by
499 size.

500

501 *Plasmid construction.*

502 Primers (Supplementary Table 5) were used to amplify the *stomatin* promoter
503 sequence by PCR from ISE6 DNA. The resulting fragment was cloned into a pTE
504 luciferase plasmid (Signosis, LR-2200) using BglIII. *Ixodes nf-y* and the active region of
505 *atf6* (amino acids 1-365) were synthesized by GenScript. *Ixodes atf6* was cloned into
506 pCMV-HA (New MCS) (gift from Christopher A. Walsh; Addgene plasmid number
507 32530) using EcoRI and EcoRV. *Ixodes nf-y* was cloned into pCMV/hygro-Negative
508 control vector (SinoBiological; CV005) using HindIII and KpnI. All constructs were
509 confirmed by sequencing (Plasmidsaurus).

510

511 *HEK 293T cell transfection.*

512 1 x 10⁶ HEK 293T cells were seeded into a 6-well plate. The next day, cells were
513 either singly or co-transfected with pCMV-ATF6-HA and pCMV-NFY-FLAG using 10 µl
514 Lipofectamine 3000, 10 µl P reagent (Fisher Scientific; L30000015), in Opti-MEM I
515 reduced-serum medium (Gibco; 31985062). After 5 hours, the medium was replaced
516 with complete DMEM and cells were incubated at 33°C, 5% CO₂ for 24 hours. Cells

517 were lysed and collected in RIPA (radioimmunoprecipitation assay; Fisher Scientific;
518 PI89901) supplemented with 1 x protease and phosphatase inhibitors
519 (ThermoScientific; 78440)^{11,12}.

520

521 *Polyacrylamide gel electrophoresis and Western blotting.*

522 Protein concentrations were determined by BCA assay (Bicinchoninic acid assay;
523 Pierce; 23225). For each sample, 20 µg of protein was separated using a 4-15% MP
524 TGX precast cassette (Bio-Rad; 4568084) at 100 V for approximately 1 hour and 30
525 minutes before being transferred to a PVDF (polyvinylidene difluoride) membrane.
526 Membranes were blocked with 5% milk in 1 x PBS-T (phosphate-buffered saline
527 containing 0.1% Tween 20) for approximately 1 hour at room temperature. All primary
528 antibodies were diluted in 5% milk, PBS-T and incubated with the blot overnight at 4°C.
529 The primary antibodies used were anti-HA anti-mouse (Invitrogen 26153; 1:1000), anti-
530 FLAG-HRP diluted (Sigma A8512; 1:2000), and anti-Actin (Sigma A2105; 1:1000).
531 Membranes were then washed 3 times with 0.5% milk, PBS-T before adding a
532 secondary antibody. Secondary antibodies included rabbit anti-mouse (Star13B; 1:2000
533 dilution) and donkey anti-rabbit (Sigma; A16023; 1:5000). Secondary antibodies were
534 incubated with membranes for 2 hours at room temperature. Membranes were then
535 washed and imaged using an ECL western blotting substrate (Enhanced
536 chemiluminescence; Fisher Scientific; P13216).

537

538 *Luciferase Reporter Assays.*

539 For the ATF6 activation assay, 1×10^4 HEK 293T cells were seeded into white-
540 walled, clear-bottom 96-well plates (Greiner Bio-One, 655098). The following day, cells
541 were transfected with 0.05 μg of the ATF6 luciferase reporter plasmid using 0.5 μl of
542 Lipofectamine 3000 in Opti-MEM I reduced-serum medium (Gibco, 31985062).
543 Transfections were allowed to proceed overnight. The following day, cells were infected
544 for 18 hours with *A. phagocytophilum* (MOI 50) or *B. burgdorferi* (MOI 200) or left
545 uninfected. Luminescence was measured the following day by adding 5 mg mL^{-1} of D-
546 Luciferin potassium salt (Promega, E1500) to each well and quantifying with a plate
547 reader. Data is represented as relative luciferase units (RLU) normalized to non-infected
548 controls \pm SEM.

549 To assess *stomatin* activation by ATF6, cells were triple-transfected with the
550 reporter plasmid containing Luciferase under control of the *stomatin* reporter and
551 plasmids expressing *Ixodes* ATF6 and NF-Y (0.05 μg of each). Luminescence was
552 measured as described above. Data is normalized to the control containing only the
553 *stomatin* reporter plasmid without ATF6 and NF-Y expression plasmids.

554

555 *Gene expression analysis of whole ticks.*

556 Gene expression profiling was performed on ticks at both larval and nymph
557 stages. Replete larvae were collected after being fed on either clean mice, an *A.*
558 *phagocytophilum*-infected mouse, or *B. burgdorferi*-infected mouse. *A.*
559 *phagocytophilum*-infected larvae were collected and maintained in an incubator for
560 either 7 days or were allowed to molt to nymphs. *B. burgdorferi*-infected larvae were
561 collected and either maintained for 14 days post-repletion or were allowed to molt to

562 nymphs. When isolating RNA, individual ticks were flash frozen in liquid nitrogen and
563 mechanically pulverized before adding TRIzol. RNA was isolated and cDNA was
564 synthesized as described above. Primers listed in Supplementary Table 5 were used to
565 measure gene expression by qRT-PCR as described above. All samples were
566 normalized to uninfected controls. Data is expressed as means \pm SEM.

567

568 *RNAi silencing and analysis of whole ticks.*

569 *I. scapularis* larvae were silenced with RNAi as previously described^{11,12}. Around
570 150 larvae were placed in a 1.5 mL tube with 40 μ l of siRNA or scrambled controls and
571 incubated overnight at 15°C. Larvae were then dried and allowed to recover overnight
572 before being placed on infected mice. Replete larvae were collected over a period of 3-5
573 days and frozen. To assess feeding efficiency, larvae were weighed in groups of three.
574 RNA was isolated from individual ticks as described above. To generate absolute
575 numbers of the target sequences, qRT-PCR was performed with a standard curve.
576 Standard curves were generated with a plasmid containing either *A. phagocytophilum*
577 *16s*, *B. burgdorferi flab*, *Ixodes β -actin*, or *Ixodes stomatin* (Supplementary Table 5).

578

579 *Cholesterol Accumulation Assays.*

580 To quantify cholesterol in tick cells, the Amplex Red Cholesterol Assay Kit
581 (Invitrogen, A12216) was used. 6.5×10^7 of ISE6 cells were seeded in T-25 tissue
582 culture flasks (Greiner Bio-one 07-000-226). The next day, the monolayer was washed
583 three times with PBS and resuspended in 1 mL of PBS. An aliquot was set aside for
584 RNA isolation and *β -actin* measurement. The rest of this sample was used for

585 cholesterol quantification. 50 μ l of each sample was added to a 96 well clear-bottom,
586 black-sided plate (Thermo Scientific, 12-566-70). Total cholesterol was quantified via
587 the Amplex Red Cholesterol Assay Kit (Invitrogen, A12216) according to the
588 manufacturer's instructions and absorbance was measured at 590 nm. A standard
589 curve was used to calculate total cholesterol concentration. Data is normalized to
590 absolute copies of *β -actin*.

591 To quantify cholesterol in *A. phagocytophilum*, 4×10^6 cells of persistently
592 infected ISE6 cells that were silenced for *stomatin* (12 μ g of siRNA or scRNA with 10 μ l
593 Lipofectamine 3000) were seeded into 6-well plates (STARSTEDT, 83.1839). 5 days
594 post-transfection cells were collected in PBS. Host cell-free *A. phagocytophilum* were
595 isolated by sonication. Briefly, cells were centrifuged at 2300 x g for 10 minutes at 4°C
596 and resuspended in 500 μ l of PBS. Samples were sonicated four times for 15 seconds
597 at an amplitude of 30V and lysates were centrifuged at 710 x g for 5 minutes to remove
598 host cell debris. The supernatant was collected and an additional spin at 2300 x g for 10
599 minutes was performed to collect *A. phagocytophilum*. Samples were resuspended in
600 200 μ l of PBS. 100 μ l was used to quantify cholesterol as described above. The
601 remaining sample was used to quantify bacteria by isolating RNA, synthesizing cDNA,
602 and quantifying *phagocytophilum 16s* by qRT-PCR. Total cholesterol was normalized to
603 *A. phagocytophilum 16s*. One well was collected in TRIzol and analyzed by qRT-PCR to
604 assess silencing efficiency.

605

606 *Statistical analysis.*

607 *In vivo* experiments used at least 10-20 ticks and *in vitro* experiments had at
608 least three to five replicates. Data was analyzed with a non-parametric Mann-Whitney
609 test or an unpaired Student's t-test respectively and expressed as means \pm SEM.
610 GraphPad Prism was used for calculations and creating graphs. Statistical significance
611 was determined by a *P* value of <0.05 .
612

613 **REFERENCES**

- 614 1. CDC. Tickborne diseases of the United States | CDC. *Centers for Disease Control*
615 *and Prevention* <https://www.cdc.gov/ticks/diseases/index.html> (2023).
- 616 2. Rosenberg, R. Vital Signs: Trends in Reported Vectorborne Disease Cases —
617 United States and Territories, 2004–2016. *MMWR Morb. Mortal. Wkly. Rep.* **67**,
618 (2018).
- 619 3. Annual statistics from the National Notifiable Diseases Surveillance System
620 (NNDSS).
621 https://wonder.cdc.gov/nndss/nndss_annual_tables_menu.asp?mmwr_year=2019.
- 622 4. Sonenshine, D. E. Range Expansion of Tick Disease Vectors in North America:
623 Implications for Spread of Tick-Borne Disease. *Int. J. Environ. Res. Public. Health*
624 **15**, 478 (2018).
- 625 5. Vector-borne diseases. [https://www.who.int/news-room/fact-sheets/detail/vector-](https://www.who.int/news-room/fact-sheets/detail/vector-borne-diseases)
626 [borne-diseases](https://www.who.int/news-room/fact-sheets/detail/vector-borne-diseases).
- 627 6. Threats, I. of M. (US) F. on M. Vector-Borne Disease Emergence and Resurgence.
628 in *Vector-Borne Diseases: Understanding the Environmental, Human Health, and*
629 *Ecological Connections: Workshop Summary* (National Academies Press (US),
630 2008).
- 631 7. Paddock, C. D., Lane, R. S., Staples, J. E. & Labruna, M. B. *CHANGING*
632 *PARADIGMS FOR TICK-BORNE DISEASES IN THE AMERICAS*. *Global Health*
633 *Impacts of Vector-Borne Diseases: Workshop Summary* (National Academies Press
634 (US), 2016).

- 635 8. *Critical Needs and Gaps in Understanding Prevention, Amelioration, and Resolution*
636 *of Lyme and Other Tick-Borne Diseases: The Short-Term and Long-Term*
637 *Outcomes: Workshop Report*. (National Academies Press, Washington, D.C., 2011).
638 doi:10.17226/13134.
- 639 9. Jongejan, F. & Uilenberg, G. The global importance of ticks. *Parasitology* **129**, S3–
640 S14 (2004).
- 641 10. Park, J. M., Oliva Chávez, A. S. & Shaw, D. K. Ticks: More Than Just a Pathogen
642 Delivery Service. *Front. Cell. Infect. Microbiol.* **11**, (2021).
- 643 11. Sidak-Loftis, L. C. *et al.* The Unfolded-Protein Response Triggers the Arthropod
644 Immune Deficiency Pathway. *mBio* **13**, e00703-22 (2022).
- 645 12. Rosche, K. L. *et al.* PERK-mediated antioxidant response is key for pathogen
646 persistence in ticks. *mSphere* **0**, e00321-23 (2023).
- 647 13. Kraskiewicz, H. & FitzGerald, U. InterfERing with endoplasmic reticulum stress.
648 *Trends Pharmacol. Sci.* **33**, 53–63 (2012).
- 649 14. Hillary, R. F. & FitzGerald, U. A lifetime of stress: ATF6 in development and
650 homeostasis. *J. Biomed. Sci.* **25**, 48 (2018).
- 651 15. O’Neal, A. J., Butler, L. R., Rolandelli, A., Gilk, S. D. & Pedra, J. H. Lipid hijacking: A
652 unifying theme in vector-borne diseases. *eLife* **9**, e61675 (2020).
- 653 16. Rosche, K. L., Sidak-Loftis, L. C., Hurtado, J., Fisk, E. A. & Shaw, D. K. Arthropods
654 Under Pressure: Stress Responses and Immunity at the Pathogen-Vector Interface.
655 *Front. Immunol.* **11**, (2021).
- 656 17. Celli, J. & Tsolis, R. M. Bacteria, the endoplasmic reticulum and the unfolded protein
657 response: friends or foes? *Nat. Rev. Microbiol.* **13**, 71–82 (2015).

- 658 18. Arensdorf, A., Diedrichs, D. & Rutkowski, T. Regulation of the transcriptome by ER
659 stress: non-canonical mechanisms and physiological consequences. *Front. Genet.*
660 **4**, (2013).
- 661 19. Wang, Y. *et al.* Activation of ATF6 and an ATF6 DNA binding site by the
662 endoplasmic reticulum stress response. *J. Biol. Chem.* **275**, 27013–27020 (2000).
- 663 20. Jumper, J. *et al.* Highly accurate protein structure prediction with AlphaFold. *Nature*
664 **596**, 583–589 (2021).
- 665 21. Varadi, M. *et al.* AlphaFold Protein Structure Database: massively expanding the
666 structural coverage of protein-sequence space with high-accuracy models. *Nucleic*
667 *Acids Res.* **50**, D439–D444 (2022).
- 668 22. Pettersen, E. F. *et al.* UCSF ChimeraX: Structure visualization for researchers,
669 educators, and developers. *Protein Sci. Publ. Protein Soc.* **30**, 70–82 (2021).
- 670 23. Kokame, K., Kato, H. & Miyata, T. Identification of ERSE-II, a New *cis*-Acting
671 Element Responsible for the ATF6-dependent Mammalian Unfolded Protein
672 Response*. *J. Biol. Chem.* **276**, 9199–9205 (2001).
- 673 24. Yoshida, H. *et al.* ATF6 Activated by Proteolysis Binds in the Presence of NF-Y
674 (CBF) Directly to the *cis*-Acting Element Responsible for the Mammalian Unfolded
675 Protein Response. *Mol. Cell. Biol.* **20**, 6755–6767 (2000).
- 676 25. Consortium, T. G. O. *et al.* Gene Ontology: tool for the unification of biology. *Nat.*
677 *Genet.* **25**, 25 (2000).
- 678 26. The Gene Ontology Consortium *et al.* The Gene Ontology knowledgebase in 2023.
679 *GENETICS* **224**, iyad031 (2023).

- 680 27. Gillespie, M. *et al.* The reactome pathway knowledgebase 2022. *Nucleic Acids Res.*
681 **50**, D687–D692 (2022).
- 682 28. Thomas, P. D. *et al.* PANTHER: Making genome-scale phylogenetics accessible to
683 all. *Protein Sci. Publ. Protein Soc.* **31**, 8 (2021).
- 684 29. Lei, Y. *et al.* Molecular mechanism of ATF6 in unfolded protein response and its role
685 in disease. *Heliyon* **10**, (2024).
- 686 30. Vekich, J. A., Belmont, P. J., Thuerauf, D. J. & Glembotski, C. C. Protein Disulfide
687 Isomerase-associated 6 is an ATF6-inducible ER Stress Response Protein that
688 Protects Cardiac Myocytes from Ischemia/Reperfusion-mediated Cell Death. *J. Mol.*
689 *Cell. Cardiol.* **53**, 259–267 (2012).
- 690 31. Dadey, D. Y. *et al.* The ATF6 pathway of the ER stress response contributes to
691 enhanced viability in glioblastoma. *Oncotarget* **7**, 2080 (2015).
- 692 32. Zhou, B. *et al.* Notch signaling pathway: architecture, disease, and therapeutics.
693 *Signal Transduct. Target. Ther.* **7**, 1–33 (2022).
- 694 33. Salzer, U., Mairhofer, M. & Prohaska, R. Stomatin: A New Paradigm of Membrane
695 Organization Emerges.
- 696 34. Abramson, J. *et al.* Accurate structure prediction of biomolecular interactions with
697 AlphaFold 3. *Nature* **630**, 493–500 (2024).
- 698 35. Blackwood, E. A. *et al.* Pharmacologic ATF6 activation confers global protection in
699 widespread disease models by reprogramming cellular proteostasis. *Nat. Commun.*
700 **10**, 187 (2019).

- 701 36. Piesman, J., Oliver, J. R. & Sinsky, R. J. Growth kinetics of the Lyme disease
702 spirochete (*Borrelia burgdorferi*) in vector ticks (*Ixodes dammini*). *Am. J. Trop. Med.*
703 *Hyg.* **42**, 352–357 (1990).
- 704 37. Browman, D. T., Hoegg, M. B. & Robbins, S. M. The SPFH domain-containing
705 proteins: more than lipid raft markers. *Trends Cell Biol.* **17**, 394–402 (2007).
- 706 38. Rungaldier, S. *et al.* Structure-function analysis of human stomatin: A mutation
707 study. *PLoS ONE* **12**, e0178646 (2017).
- 708 39. Xiong, Q., Lin, M. & Rikihisa, Y. Cholesterol-Dependent Anaplasma
709 phagocytophilum Exploits the Low-Density Lipoprotein Uptake Pathway. *PLOS*
710 *Pathog.* **5**, e1000329 (2009).
- 711 40. Strauss, K. *et al.* Exosome Secretion Ameliorates Lysosomal Storage of Cholesterol
712 in Niemann-Pick Type C Disease. *J. Biol. Chem.* **285**, 26279–26288 (2010).
- 713 41. Matys, V. *et al.* TRANSFAC® and its module TRANSCompel®: transcriptional gene
714 regulation in eukaryotes. *Nucleic Acids Res.* **34**, D108–D110 (2006).
- 715 42. Zhang, Q. *et al.* hTFtarget: A Comprehensive Database for Regulations of Human
716 Transcription Factors and Their Targets. *Genomics Proteomics Bioinformatics* **18**,
717 120–128 (2020).
- 718 43. Chakrabarti, A., Chen, A. W. & Varner, J. D. A review of the mammalian unfolded
719 protein response. *Biotechnol. Bioeng.* **108**, 2777–2793 (2011).
- 720 44. Meex, S. J. R. *et al.* The ATF6-Met[67]Val Substitution Is Associated With Increased
721 Plasma Cholesterol Levels. *Arterioscler. Thromb. Vasc. Biol.* **29**, 1322–1327 (2009).

- 722 45. Zhang, Q. *et al.* hTFtarget: A Comprehensive Database for Regulations of Human
723 Transcription Factors and Their Targets. *Genomics Proteomics Bioinformatics* **18**,
724 120–128 (2020).
- 725 46. Shaw, D. K. *et al.* Vector Immunity and Evolutionary Ecology: The Harmonious
726 Dissonance. *Trends Immunol.* **39**, 862–873 (2018).
- 727 47. Simons, K. & Sampaio, J. L. Membrane Organization and Lipid Rafts. *Cold Spring*
728 *Harb. Perspect. Biol.* **3**, a004697 (2011).
- 729 48. Goldmann, M. *et al.* The Lipid Raft-Associated Protein Stomatin Is Required for
730 Accumulation of Dectin-1 in the Phagosomal Membrane and for Full Activity of
731 Macrophages against *Aspergillus fumigatus*. *mSphere* **8**, e00523-22 (2023).
- 732 49. Kim, J.-H., Rhee, J.-K., Ahn, D.-G., Kim, K. P. & Oh, J.-W. Interaction of stomatin
733 with hepatitis C virus RNA polymerase stabilizes the viral RNA replicase complexes
734 on detergent-resistant membranes. *J. Microbiol. Biotechnol.* **24**, 1744–1754 (2014).
- 735 50. Huang, W., Xiong, Q., Lin, M. & Rikihisa, Y. *Anaplasma phagocytophilum* Hijacks
736 Flotillin and NPC1 Complex To Acquire Intracellular Cholesterol for Proliferation,
737 Which Can Be Inhibited with Ezetimibe. *mBio* **12**, e02299-21 (2021).
- 738 51. Xiong, Q., Lin, M., Huang, W. & Rikihisa, Y. Infection by *Anaplasma*
739 *phagocytophilum* Requires Recruitment of Low-Density Lipoprotein Cholesterol by
740 Flotillins. *mBio* **10**, 10.1128/mbio.02783-18 (2019).
- 741 52. Wang, L., Lin, M., Hou, L. & Rikihisa, Y. *Anaplasma phagocytophilum* effector EgeA
742 facilitates infection by hijacking TANGO1 and SCFD1 from ER–Golgi exit sites to
743 pathogen-occupied inclusions. *Proc. Natl. Acad. Sci.* **121**, e2405209121 (2024).

- 744 53. Yoshikawa Y, Sugimoto K, Ochiai Y, & Ohashi N. Intracellular proliferation of
745 *Anaplasma phagocytophilum* is promoted via modulation of endoplasmic reticulum
746 stress signaling in host cells. *Microbiol. Immunol.* **64**, 270–279 (2020).
- 747 54. Shaw, D. K. *et al.* Infection-derived lipids elicit an immune deficiency circuit in
748 arthropods. *Nat. Commun.* **8**, 14401 (2017).
- 749 55. Decreased Infectivity in *Borrelia burgdorferi* Strain B31 Is Associated with Loss of
750 Linear Plasmid 25 or 28-1 | Infection and Immunity.
751 <https://journals.asm.org/doi/full/10.1128/iai.69.1.446-455.2001>.
- 752 56. Waterhouse, A. M., Procter, J. B., Martin, D. M. A., Clamp, M. & Barton, G. J.
753 Jalview Version 2—a multiple sequence alignment editor and analysis workbench.
754 *Bioinformatics* **25**, 1189–1191 (2009).
- 755 57. R Core Team. R: A Language and Environment for Statistical Computing. R
756 Foundation for Statistical Computing (2021).
- 757 58. RStudio Team. *RStudio: Integrated Development Environment for R*. (RStudio,
758 PBC, 2022).
- 759 59. Sayers, E. W. *et al.* Database resources of the national center for biotechnology
760 information. *Nucleic Acids Res.* **50**, D20–D26 (2022).
- 761 60. Pagès, H., Aboyoun, P., Gentleman, R. & DebRoy, S. Biostrings: Efficient
762 manipulation of biological strings. (2021).
- 763 61. Charif, D. & Lobry, J. R. SeqinR 1.0-2: a contributed package to the R project for
764 statistical computing devoted to biological sequences retrieval and analysis. in
765 *Structural approaches to sequence evolution: Molecules, networks, populations*

- 766 (eds. Bastolla, U., Porto, M., Roman, H. E. & Vendruscolo, M.) 207–232 (Springer
767 Verlag, New York, 2007).
- 768 62. Wickham, H. *Stringr: Simple, Consistent Wrappers for Common String Operations*.
769 (2023).
- 770 63. Chang, W. *et al. Shiny: Web Application Framework for R*. (2024).
- 771 64. Winter, D. J. rentrez: an R package for the NCBI eUtils API. *R J.* **9**, 520–526 (2017).
- 772 65. Hahsler, M. & Anurag, N. *rBLAST: R Interface for the Basic Local Alignment Search*
773 *Tool*. (2024).
- 774 66. Yu, G. *Enrichplot: Visualization of Functional Enrichment Result*. (2023).
- 775
- 776

777 **FIGURE LEGENDS**

778 **Figure 1. ATF6 is induced by tick-borne pathogens during infection and supports**
779 **vector colonization.** (A) HEK 293T cells were transfected with an ATF6 luciferase
780 reporter plasmid. Transfected cells were infected with *A. phagocytophilum* (MOI 50) or
781 *B. burgdorferi* (MOI 200) for 18 hours and normalized to no infection (-). RLU is relative
782 luminescence units. (B) Schematic depicting ATF6 activation. (C-D) Gene expression of
783 *atf6* in *I. scapularis* larvae rested for 7 days after feeding on *Anaplasma*-infected mice
784 (C) and rested for 14 days after feeding on *Borrelia*-infected mice (D). Expression was
785 assessed via qRT-PCR. Each data point is representative of 1 larva. (-) is no infection.
786 *A.p.* is *A. phagocytophilum*. *B.b.* is *B. burgdorferi*. (E) RNAi knockdown of *atf6* in ISE6
787 cells for 5 days and infected with *A. phagocytophilum* (MOI 50). scRNA, scrambled
788 RNA; siRNA, small interfering RNA. Experiments are representative of at least 2
789 experimental replicates. *P < 0.05.

790

791 **Supplemental Figure 1. *I. scapularis* ATF6 sequence alignment and structural**
792 **prediction with AlphaFold.** (A) Human and *I. scapularis* ATF6 protein sequences were
793 aligned and visualized with Jalview. Shaded amino acid residues indicate conservation
794 and percent identity between the two proteins. DNA binding residues are highlighted in
795 gold. *H.s.* is *Homo sapiens*. *I.s.* is *I. scapularis*. (B) *I. scapularis* ATF6 predicted by
796 AlphaFold. Color of each residue represents the model confidence score, pLDDT. Blue
797 indicates regions predicted with high confidence. Yellow to orange indicates regions of
798 low confidence.

799

800 **Figure 2. Predicting the ATF6 regulatory network in ticks.** (A) The *I. scapularis*
801 ATF6 (orange) predicted with AlphaFold has a conserved DNA binding domain
802 compared to the human ortholog (green). (B) A portion of the bZIP domain and the DNA
803 binding residues on ATF6 are visualized. (C) Schematic of the developed R script. (D)
804 Comparison of genes predicted to be regulated by ATF6 from the *I. scapularis*, *D.*
805 *melanogaster*, and *H. sapiens*. (E) GO terms and Reactome pathways represented in
806 predicted ATF6-regulated genes from *I. scapularis* genome.

807

808 **Supplementary Figure 2. Predicted ATF6 regulatory network across organisms.**
809 GO enrichment analysis comparison between predicted ATF6-regulated genes from *I.*
810 *scapularis*, *D. melanogaster*, and *H. sapiens*.

811

812 **Figure 3. ATF6 upregulates *stomatin* during infection in ticks.** (A) The AlphaFold3
813 predicted DNA-protein complex with *I. scapularis* nATF6 (tan) and the predicted
814 promoter of *stomatin* (teal). The ATF6 binding site is highlighted in yellow and DNA
815 binding residues highlighted in purple. (B-C) *stomatin* expression quantified from (B)
816 ISE6 cells treated with 5 μ M-50 μ M of AA147 for 24 hours and (C) ISE6 cells
817 transfected with siRNA targeting *atf6* or a scrambled control. (D) HEK 293T cells were
818 co-transfected with plasmids constitutively expressing *I. scapularis* nATF6, *I. scapularis*
819 NF-Y, and a luciferase reporter plasmid with the *stomatin* promoter. Luciferase activity
820 was normalized to the control containing only the luciferase reporter plasmid. RLU is
821 relative luminescence units. (E-F) Gene expression of larvae rested for 7 days after
822 being fed on *Anaplasma*-infected mice (E) or rested for 14 days after being fed on *B.*

823 *burgdorferi*-infected mice (F). (G) *stomatin* gene expression from unfed, infected *I.*
824 *scapularis* nymphs. *A.p.* is *A. phagocytophilum*. *B.b.* is *B. burgdorferi*. Expression
825 assessed via qRT-PCR. *P < 0.05.

826

827 **Supplementary Figure 3. Structural interaction of ATF6 and cell viability post**

828 **AA147 treatment.** (A) AlphaFold3 prediction of ATF6 dimer binding to *stomatin*
829 promoter. Color of each residue represents the model confidence score, pLDDT. Blue
830 indicates regions predicted with high confidence. Yellow to orange indicates regions of
831 low confidence. (B) Cell viability measured for ISE6 cells treated with 5 μ M-50 μ M of
832 AA147 for 24 hours.

833

834 **Supplementary Figure 4. ATF6 schematic and recombinant protein expression**

835 **with NF-Y.** (A) ATF6 linear structure. Green bars indicate glycosylation sites at 98-102,
836 216-220, 334-338, 470-474, 621-625. Purple bars indicate S1 and S2 protease sites at
837 412-415 and 382-385 respectively. (B) Immunoblot against HEK 293T cells transfected
838 with FLAG-tagged pCMV-NF-Y and HA-tagged pCMV-ATF6 (C) HEK 293T cells were
839 co-transfected with an ATF6 luciferase reporter plasmid and plasmids constitutively
840 expressing *I. scapularis* ATF6 and *I. scapularis* NF-Y. Luciferase activity was
841 normalized to the control containing only the luciferase reporter plasmid. RLU is relative
842 luminescence units.

843

844 **Figure 4. Stomatin supports infection by facilitating *A. phagocytophilum***

845 **cholesterol uptake.** (A) ISE6 cells were transfected with siRNA or a scrambled control.

846 Cells were infected with *A. phagocytophilum* (MOI 50) for 18 hours. (B) siRNA-treated
847 or scrambled control-treated larvae were fed on *A. phagocytophilum*-infected mice.
848 Each data point is representative of 1 larva. Open and closed dots represent
849 experimental replicates 1 and 2. Gene silencing and bacterial burden were measured by
850 qRT-PCR. (C) AlphaFold-predicted *I. scapularis* Stomatin with SPFH domain
851 highlighted in blue and cholesterol binding domains highlighted in pink. (D) Total
852 cholesterol quantified from *A. phagocytophilum*-infected ISE6 compared to uninfected
853 cells (-). Each dot represents an experimental replicate. (E) Cholesterol quantified from
854 cells treated with silencing RNAs targeting *stomatin* or scrambled controls. (F)
855 Cholesterol quantified in *A. phagocytophilum* grown in *stomatin*-depleted ISE6 tick cells.
856 Gene silencing was measured by qRT-PCR. scRNA, scrambled RNA; siRNA, small
857 interfering RNA. Experiments are representative of at least 2 experimental replicates. *P
858 < 0.05.

859

860 **Supplemental Figure 5. *I. scapularis* Stomatin sequence alignment and structural**
861 **prediction with AlphaFold.** (A) Human and *I. scapularis* Stomatin protein sequences
862 were aligned and visualized with Jalview. Shaded amino acid residues indicate
863 conservation and percent identity between the two proteins. *H.s.* is *Homo sapiens*. *I.s.* is
864 *I. scapularis*. (B) *I. scapularis* Stomatin predicted by AlphaFold. Color of each residue
865 represents the model confidence score, pLDDT. Blue indicates regions predicted with
866 high confidence. Yellow to orange indicates regions of low confidence. (C) Predicted *I.*
867 *scapularis* Stomatin (indigo) aligned with human Stomatin (magenta). (D) *I. scapularis*
868 Stomatin sequence with highlighted cholesterol binding domains. Protein sequence

869 visualized with Jalview. The region in blue indicates the conserved SPFH domain.
870 Cholesterol binding domains, CRAC (purple) and CARC (teal) are highlighted. (E)
871 Supporting information for Fig 4F showing *stomatin* silencing levels compared to the
872 scrambled control. scRNA, scrambled RNA; siRNA, small interfering RNA.

873

874 **Figure 5. ATF6 supports arthropod infection through Stomatin-regulated**

875 **cholesterol delivery to the pathogen.** (A) Infection activates ATF6 which translocates
876 to the nucleus and upregulates *stomatin* expression. Stomatin regulates cholesterol
877 distribution in the cell and to the *Anaplasma* containing vacuole for growth and survival
878 in ticks. (B) ArthroQuest was used to identify organisms containing ATF6 binding sites
879 in the promoter regions of Stomatin orthologs. Stomatin orthologs were identified using
880 the *Ixodes* protein sequence. Green checkmarks indicate that the top ortholog contains
881 an ATF6 binding site in the promoter region. Yellow checkmarks indicate that a
882 significant ortholog hit contains an ATF6 binding site in the promoter region. Red “X”
883 indicates all BLAST hits lack an ATF6 binding site.

884

885 **ACKNOWLEDGEMENTS**

886 We are grateful to Ulrike Munderloh (University of Minnesota) for providing ISE6 tick cell
887 lines, Jon Skare (Texas A&M Health Science Center) for providing *B. burgdorferi* B31
888 (MSK5), Skandha Nadarajah, Ryan Driskell, and the Veterinary Information Systems
889 team (Washington State University) for their assistance with making ArthroQuest
890 publicly available, Ryan Vosbigian (University of Idaho) for his guidance on R
891 programming, Biodefense and Emerging Infectious Diseases Resources and Oklahoma
892 State University for *Ixodes scapularis* ticks. The Addgene plasmid 32530 was a gift from
893 Christopher A. Walsh. Schematics in Fig 1 and 7 were created with BioRender.

894

895 **Funding**

896 This work is supported by the National Institutes of Health (R21AI148578,
897 R21AI139772, and R01AI162819 to D.K.S.), the WSU Intramural CVM grants program
898 funded by the National Institute of Food and Agriculture (to D.K.S.), and Washington
899 State University, College of Veterinary Medicine. K.A.V is a trainee supported by an
900 Institutional T32 Training Grant from the National Institute of Allergy and Infectious
901 Diseases (T32GM008336). Additional support to K.A.V came from the Achievement
902 Rewards for College Scientists (ARCS) Foundation Fellowship, Veterinary Microbiology
903 and Pathology Excellence in Research Graduate Student Fellowship, Kraft Graduate
904 Scholarship funded by Dr. James and Mrs. Lillian Kraft, and the Ron and Sheila Pera
905 Scholarship. E.A.F. is a trainee supported by an Institutional T32 Training Grant from
906 the National Institute of Allergy and Infectious Diseases (T32AI007025). E.R.-Z. is a
907 trainee supported by an Institutional Training Grant MIRA R25 ESTEEMED from the

908 National Institute of Biomedical Imaging and Bioengineering (R25EB027606). The
909 content is solely the responsibility of the authors and does not necessarily represent the
910 official views of the National Institute of Allergy and Infectious Diseases or the National
911 Institutes of Health.

912

913 **Author Contributions**

914 K.A.V and D.K.S. designed the study. K.A.V., S.J.W., K.L.R., E.A.F, E.R-Z., and D.K.S.
915 performed experiments. K.A.V. and E.A.S. developed ArthroQuest. K.A.V. and D.K.S.
916 analyzed data. All authors provided intellectual input into the study. K.A.V., S.J.W., and
917 D.K.S. wrote the manuscript. All authors contributed to editing.

Figure 1. ATF6 is induced by tick-borne pathogens during infection and supports vector colonization

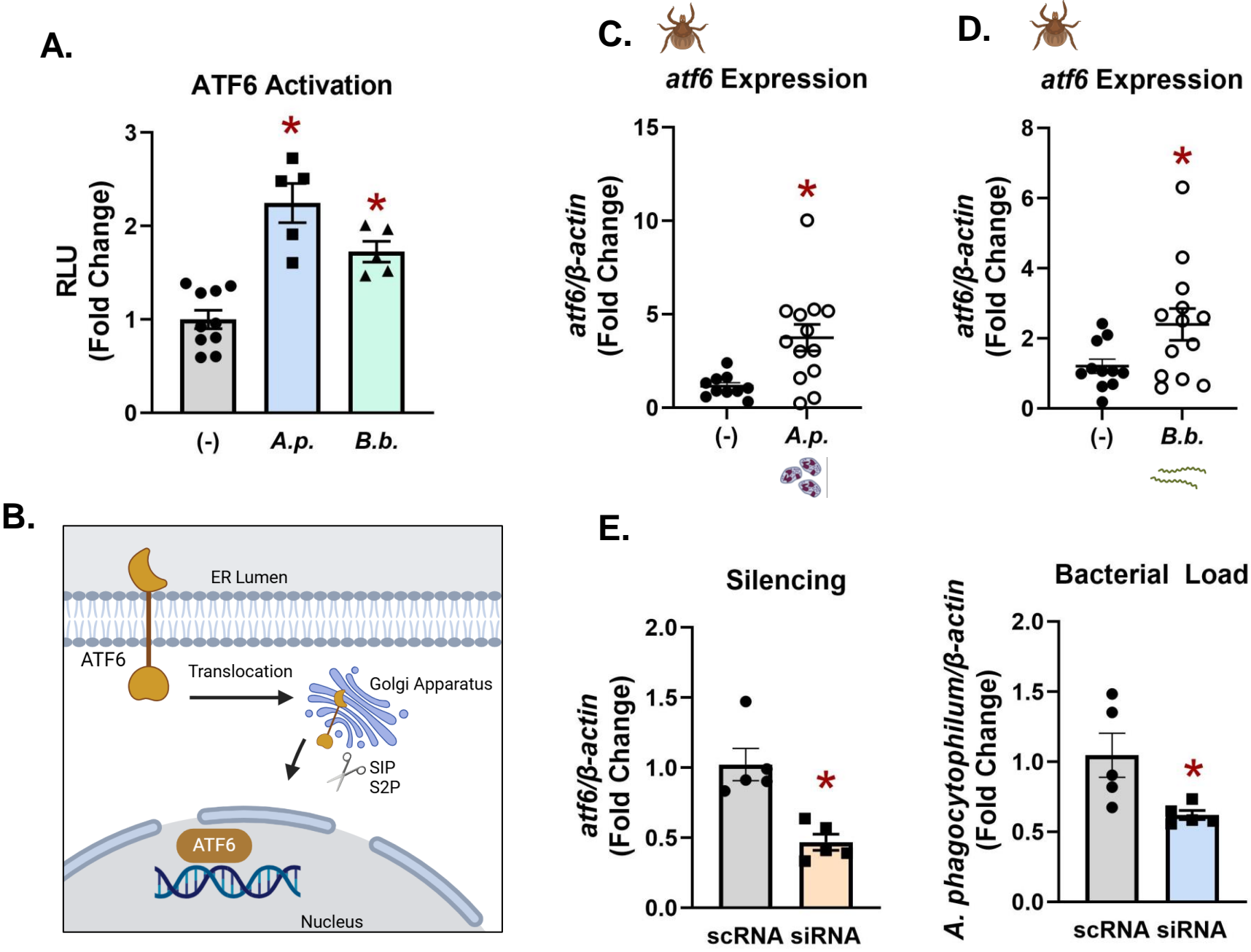


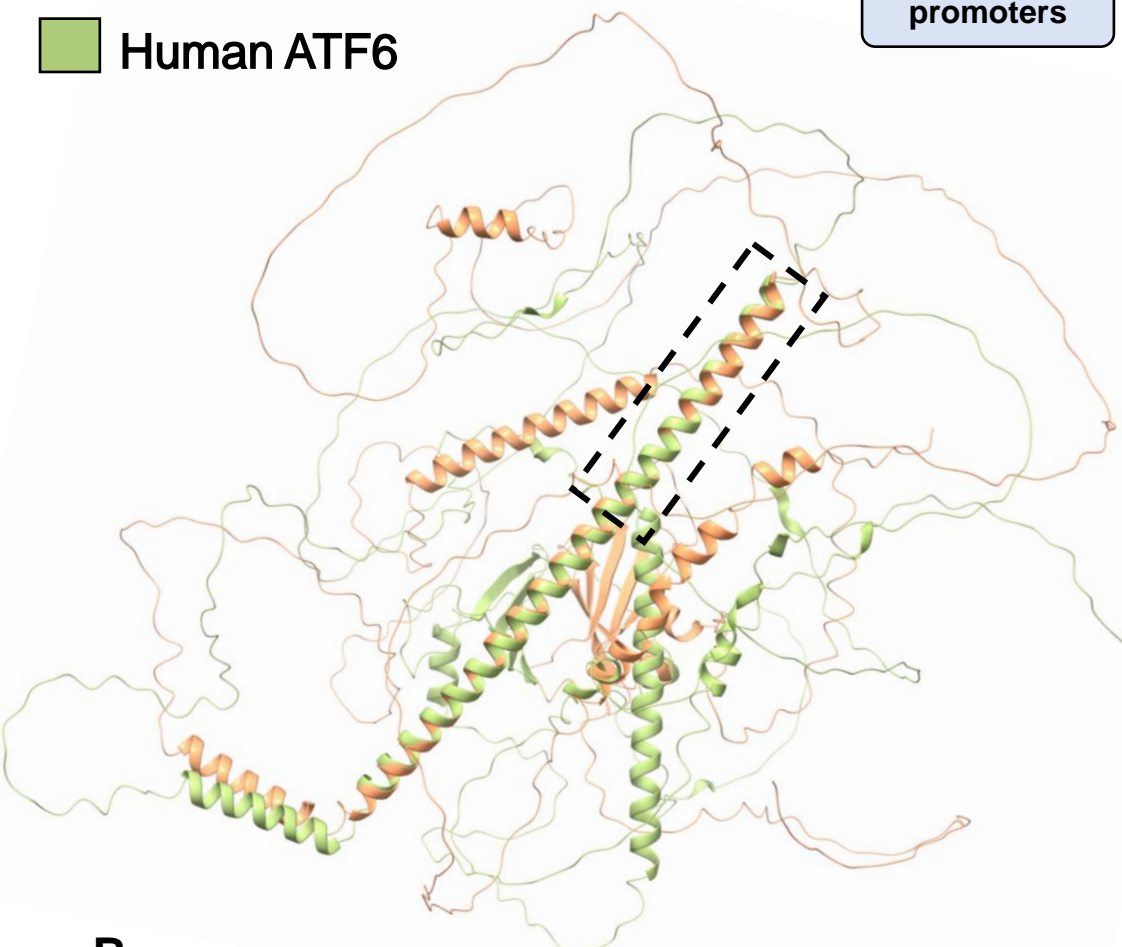


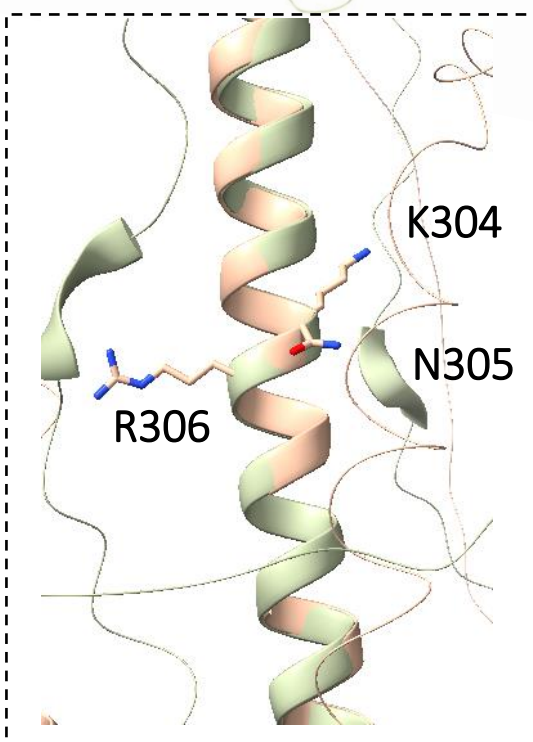
Figure 2. Predicting the ATF6 regulatory network in ticks.

A.

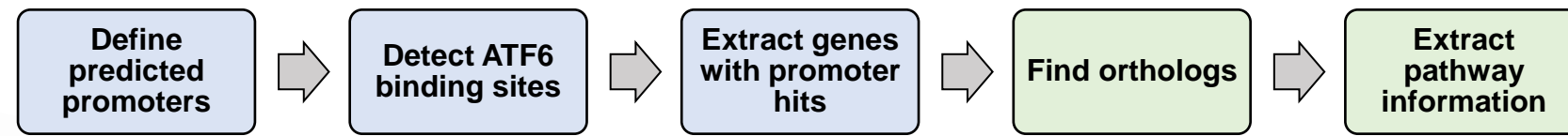
 *I. scapularis* ATF6
 Human ATF6



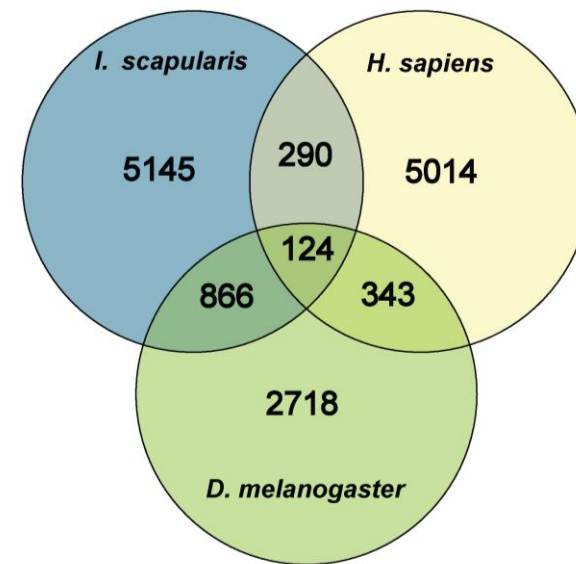
B.



C.



D.



E.

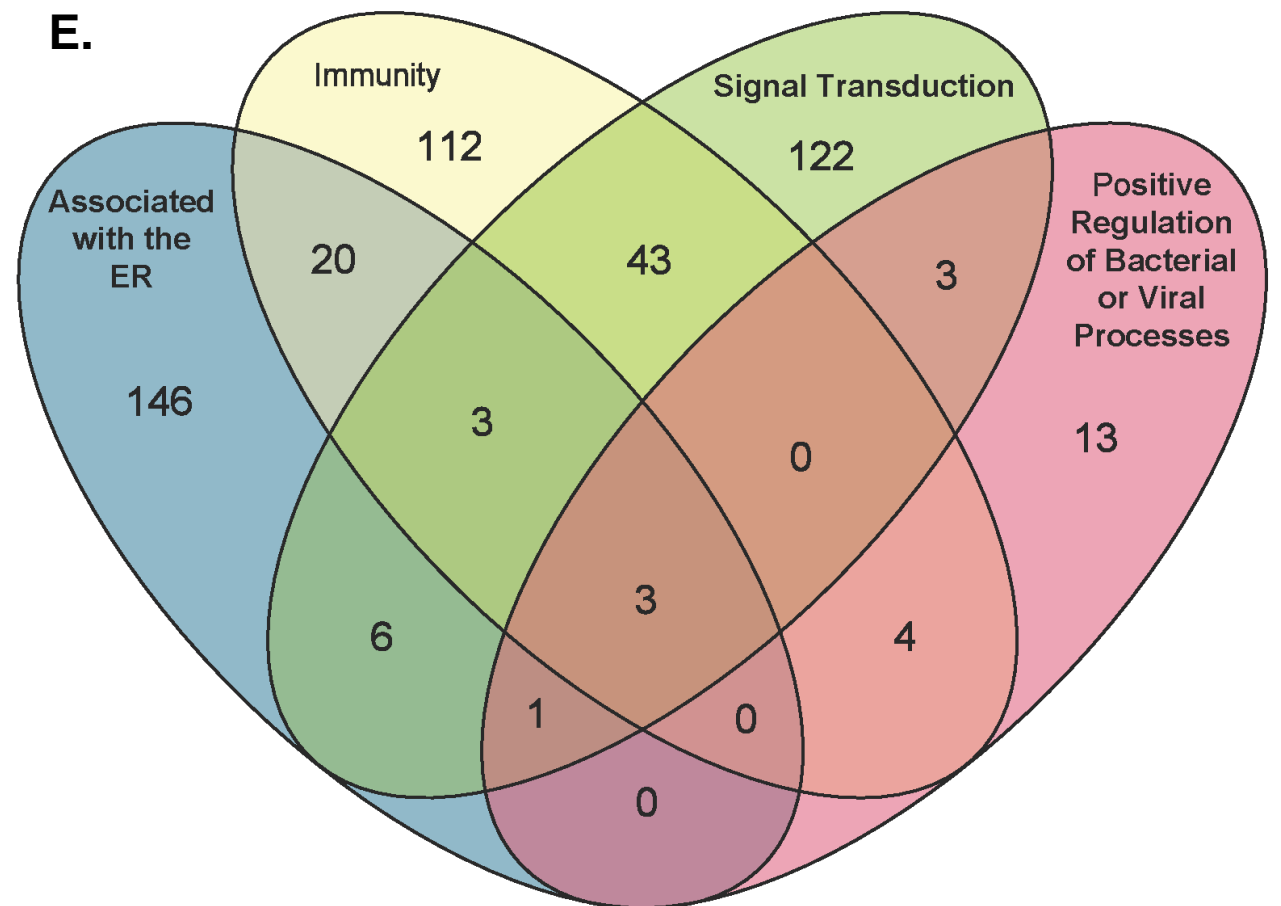


Figure 3. ATF6 upregulates *stomatin* during infection in ticks.

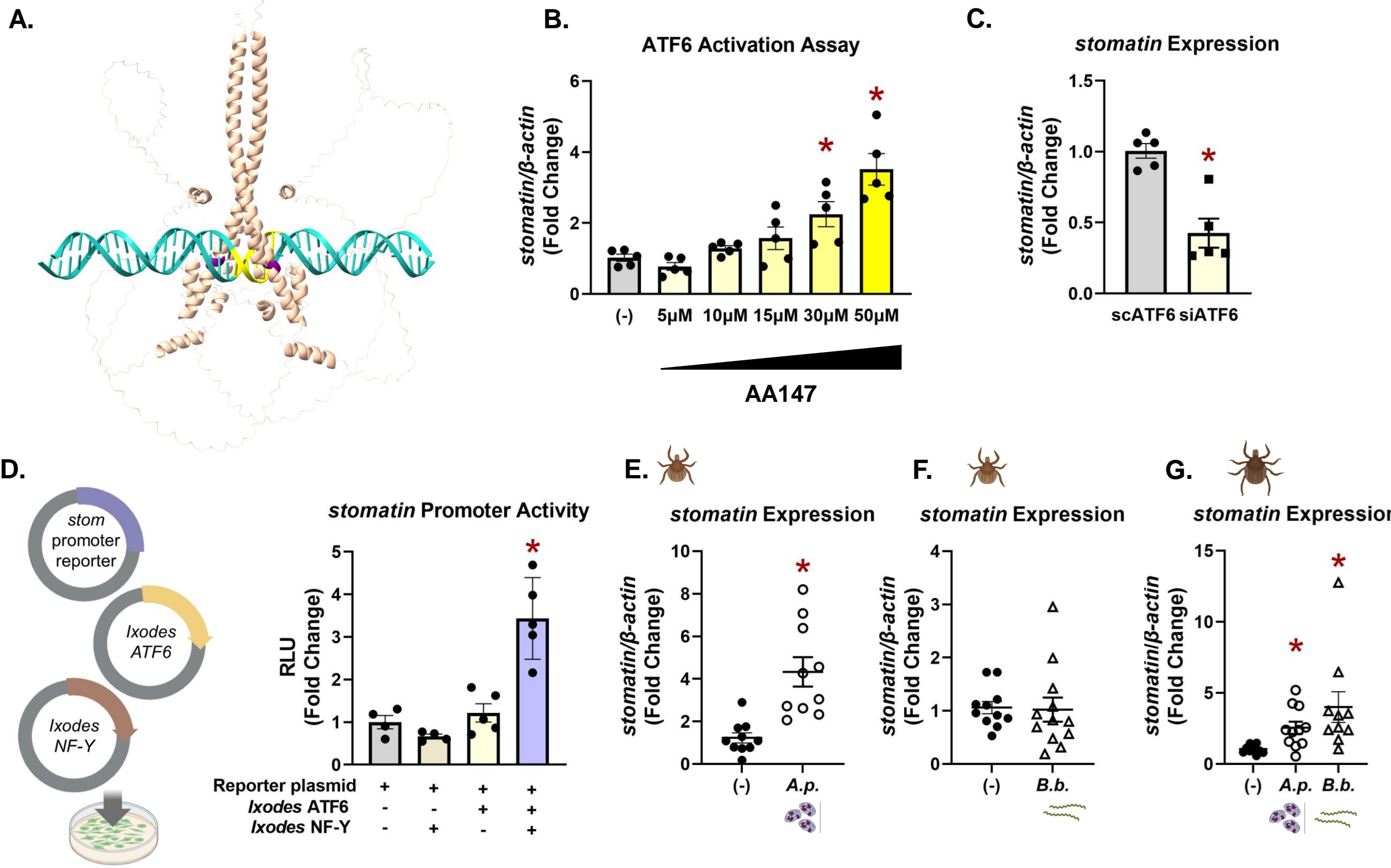


Figure 4: Stomatin supports infection by facilitating *A. phagocytophilum* cholesterol uptake.

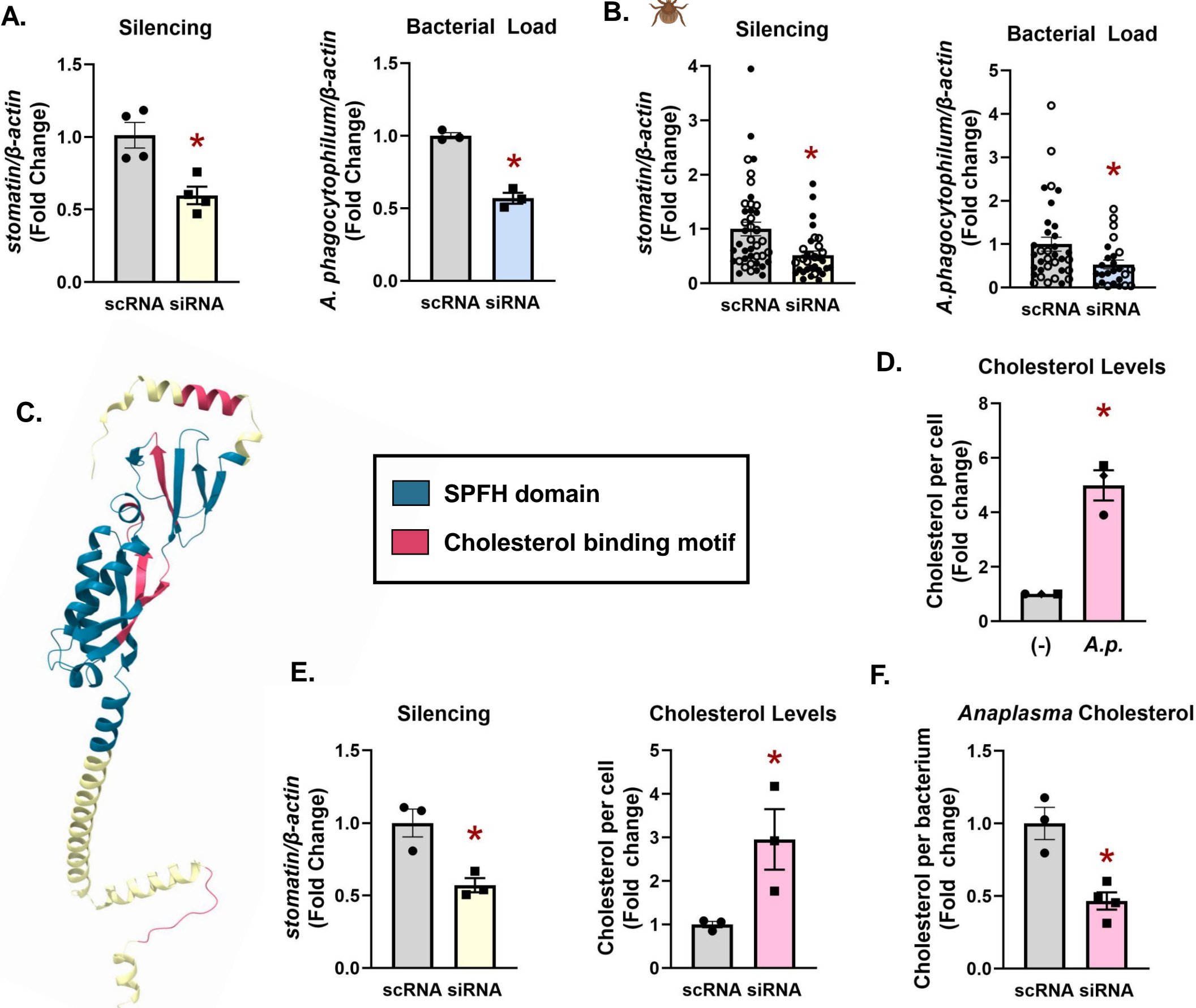
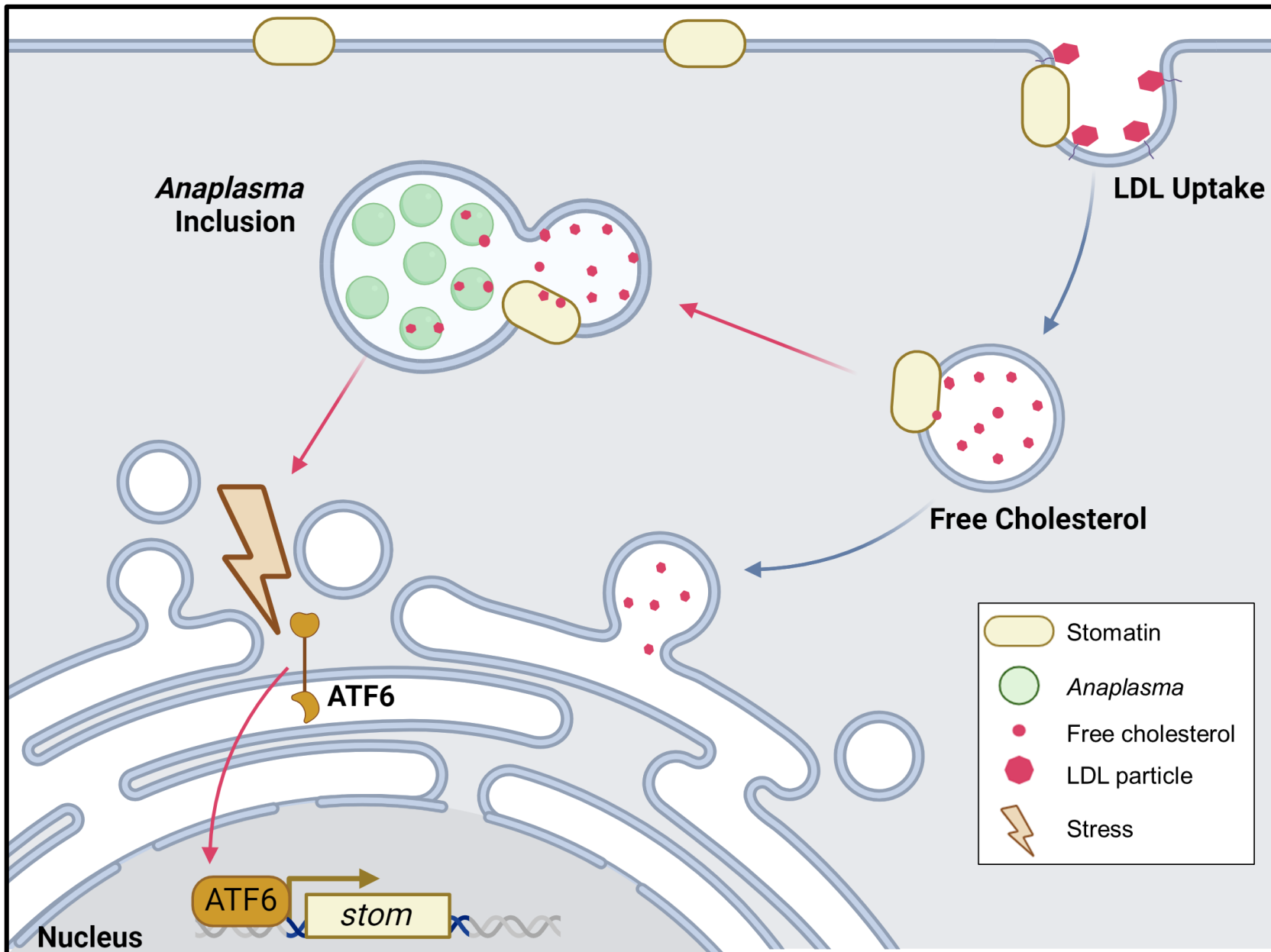


Figure 5. ATF6 supports arthropod infection through Stomatin-regulated cholesterol delivery to the pathogen.

A.



B.

ArthoQuest ATF6 binding site search		
	<i>Ixodes scapularis</i>	✓
	<i>Dermacentor andersoni</i>	✓
	<i>Dermacentor silvarum</i>	✓
	<i>Rhipicephalus appendiculatus</i>	✓
	<i>Anopheles gambiae</i>	✓
	<i>Lutzomyia longipalpis</i>	✓
	<i>Amblyomma americanum</i>	✓
	<i>Dermacentor albipictus</i>	✓
	<i>Rhipicephalus microplus</i>	✓
	<i>Rhipicephalus sanguineus</i>	✓
	<i>Ixodes persulcatus</i>	✓
	<i>Haemaphysalis longicornis</i>	✓
	<i>Hyalomma asiaticum</i>	✓
	<i>Ornithodoros turicata</i>	✓
	<i>Aedes aegypti</i>	✓
	<i>Leptotrombidium deliense</i>	✓
	<i>Phlebotomus argentipes</i>	✓
	<i>Drosophila melanogaster</i>	✓
	<i>Ctenocephalides felis</i>	✗
	<i>Pediculus humanus corporis</i>	✗
	<i>Phlebotomus papatasi</i>	✗
	<i>Homo sapiens</i>	✗